Title

Functional maturation of hPSC-derived forebrain interneurons requires an extended timeline and mimics human neural development.

Journal

Cell stem cell, 12(5)

ISSN

1934-5909

Authors

Nicholas, Cory R
Chen, Jiadong
Tang, Yunshuo
et al.

Publication Date

2013-05-01

DOI

10.1016/j.stem.2013.04.005

Peer reviewed

Published in final edited form as:
Cell Stem Cell. 2013 May 2; 12(5): 573–586. doi:10.1016/j.stem.2013.04.005.

Functional maturation of hPSC-derived forebrain interneurons requires an extended timeline and mimics human neural development

Cory R. Nicholas[1,a], **Jiadong Chen**[1,a], **Yunshuo Tang**[2], **Derek G. Southwell**[2,c], **Nadine Chalmers**[1], **Daniel Vogt**[3], **Christine M. Arnold**[2], **Ying-Jiun J. Chen**[3], **Edouard G. Stanley**[5,6], **Andrew G. Elefanty**[5,6], **Yoshiki Sasai**[4], **Arturo Alvarez-Buylla**[2,b], **John L.R. Rubenstein**[3,b], and **Arnold R. Kriegstein**[1,b]

[1]The Eli and Edythe Broad Center of Regeneration Medicine and Stem Cell Research, Department of Neurology, University of California, San Francisco, CA 94143, USA

[2]The Eli and Edythe Broad Center of Regeneration Medicine and Stem Cell Research, Department of Neurological Surgery, University of California, San Francisco, CA 94143, USA

[3]Department of Psychiatry and the Nina Ireland Laboratory of Developmental Neurobiology, University of California, San Francisco, CA 94158, USA

[4]Organogenesis and Neurogenesis Group, RIKEN Center for Developmental Biology, Kobe 650-0047, Japan

[5]The Murdoch Children's Research Institute, The Royal Children's Hospital, Parkville, Victoria 3052, Australia

[6]Monash Immunology and Stem Cell Laboratories (MISCL), Monash University, Clayton, Victoria 3800, Australia

SUMMARY

Directed differentiation from human pluripotent stem cells (hPSCs) has seen significant progress in recent years. Most differentiated populations, however, exhibit immature properties of an early embryonic stage, raising concerns about their ability to model and treat disease. Here, we report the directed differentiation of hPSCs into medial ganglionic eminence (MGE)-like progenitors and their maturation into forebrain type interneurons. We find that early stage progenitors progress via a radial glial-like stem cell enriched in the human fetal brain. Both in vitro and post-transplantation into the rodent cortex, the MGE-like cells develop into GABAergic interneuron subtypes with mature physiological properties along a prolonged intrinsic timeline of up to seven months, mimicking endogenous human neural development. MGE-derived cortical interneuron deficiencies are implicated in a broad range of neurodevelopmental and degenerative disorders, highlighting the importance of these results for modeling human neural development and disease.

Correspondence: kriegsteina@stemcell.ucsf.edu. [b]Co-corresponding authors.
[a]Authors contributed equally
[c]Present address: Department of Neurosurgery, Stanford University, Stanford, CA 94305, USA

SUPPLEMENTAL INFORMATION

Supplemental information for this article includes seven figures, three movies, four tables, and Supplemental Experimental Procedures and can be found with this article online.

INTRODUCTION

In contrast to excitatory (glutamatergic) cortical pyramidal neurons that project long distances, inhibitory (GABAergic) cortical interneurons make local synapses and are essential for maintaining the balanced activity of neural circuits (Markram et al., 2004). Most cortical interneurons are born in the MGE of the developing ventral telencephalon at mid-gestation and subsequently undergo tangential migration into the neocortex (Anderson et al., 2001; Wichterle et al., 2001). During late gestational to early post-natal stages, nascent interneuron precursors gradually develop into extremely diverse subtypes of GABAergic interneurons that can be classified by their morphology, expression of neuropeptide and/or calcium binding protein subtype markers, and intrinsic physiological membrane properties (Figure 1A) (Markram et al., 2004). Interneuron maturation occurs with the progressive acquisition of features including: increasing cell size and branching of processes, expression of subtype markers, formation of GABAergic synapses, an ability to fire high frequency trains of action potentials, and the development of more mature electrophysiological properties (Le Magueresse and Monyer, 2013).

Deficiencies in subtypes of interneurons, and resulting excitatory/inhibitory imbalances, have been associated with many neuro-developmental and degenerative disorders such as epilepsy, schizophrenia, autism, and Alzheimer's disease (Chao et al., 2010; Cheah et al., 2012; Cobos et al., 2005; Fazzari et al., 2010; Verret et al., 2012). The ability to derive mature subtypes of human interneurons from patients could provide a basis for studying the etiology as well as the potential therapeutic targets for diseases of interneuron dysfunction.

In this study, we investigate the maturation of hPSC- [human embryonic stem cell (hESC) and human induced pluripotent stem cell (hiPSC)] -derived MGE-like progenitors into functional GABAergic interneuron subtypes. Prior studies have reported the differentiation of various neural lineages from hPSCs, including ventral forebrain-like precursor cells (Elkabetz et al., 2008; Goulburn et al., 2011; Kim et al., 2011; Li et al., 2009; Ma et al., 2012; Watanabe et al., 2007). However, aside from two recent reports studying cortical-like excitatory projection neurons (Espuny-Camacho et al., 2013; Shi et al., 2012), there has been little focus on the maturation of hPSC-derived progenitor cells into functional neuronal subtypes that develop advanced physiological properties. Here, we use cell morphology, global gene expression profiling, subtype marker expression, and electrophysiological analyses to demonstrate mature features of interneuron subtypes during their protracted functional maturation from hPSCs. We find that mature hPSC-derived interneurons fire subtype-specific trains of action potentials, receive synaptic inputs, generate GABAergic-exclusive synaptic output, and functionally integrate post-injection into the rodent cortex. Moreover, we find that stem cell-derived interneurons acquire these mature features according to an intrinsic developmental timeline shared with endogenous human interneuron subtypes.

RESULTS

hPSC-derived Telencephalic MGE-like Identity

To facilitate the identification of hPSC-derived NKX2.1+ cells, we used the HES-3 hESC line (HES-3 *NKX2.1*$^{GFP/w}$) with a GFP knock-in construct inserted into the second exon of *NKX2.1* (Goulburn et al., 2011). NKX2.1 expression marks ventral forebrain-specific identity in the developing nervous system, including telencephalic MGE, pre-optic area (POA), septum, and diencephalic hypothalamus. In combination with dual-SMAD (SB431542 and BMPRIA-Fc), ROCK (Y27632), and WNT (DKK1) inhibition (Chambers et al., 2009; Li et al., 2009; Watanabe et al., 2007), we found that optimization of early SHH

pathway activation (purmorphamine) and B-27 supplementation enabled highly efficient and reproducible ventral forebrain-like differentiation from hESCs. The average *NKX2.1*-GFP+ efficiency on day 20-30 post-differentiation was 74.9 ±2.1% (n=25 independent differentiation experiments). We also found that additional hESC lines, including cGMP-matched ESI-17, 35, 51, 53 (Biotime), and H9 (WiCell), and an adult melanocyte-derived hiPSC line, differentiated into NKX2.1+ MGE-like cells at a similar efficiency. The optimized B27 + five factor (B27+5F) method is outlined in Figure 1B, and is described in detail in Figure S1 and the Supplemental Experimental Procedures.

To determine the regional identity of the *NKX2.1*-GFP+ cells, we performed a 50-day time course of suspension embryoid body (sEB) differentiation and immunostaining analysis for markers of forebrain development (Figures S2 and S3). We detected robust *NKX2.1*-GFP expression by day 10 of differentiation that co-localized with NKX2.1 protein and was expressed throughout the time course. In contrast, PAX6, a marker of dorsal telencephalic neural progenitors, was not detected. Telencephalon marker, FOXG1, was found in most cells by day 20 and remained highly expressed. In opposition to this trend, NKX2.2 expression, a marker of hypothalamus and more ventrocaudal regions, was primarily only expressed between days 10-20. Interestingly, transient appearance of NKX2.2+ ventral diencephalic-like cells may represent a stage of early forebrain development prior to the emergence of the FOXG1+ ventral telencephalon (Shimamura and Rubenstein, 1997). Additional ventral telencephalic progenitor markers, OLIG2 and ASCL1 (MASH1), were induced by day 20-30. By 30 days, sEBs expressed the migratory neuronal marker, doublecortin (DCX), and the neurotransmitter, GABA. We did not detect the hypothalamic marker RAX or cholinergic neuron marker CHAT. Therefore, the hPSC-derived *NKX2.1*-GFP+ cells represented a telencephalic MGE-like GABAergic neuronal lineage. A summary of marker expression during sEB culture is provided (Table S1).

hPSC-derived MGE-like Progenitors Exhibited VZ and SVZ Radial Glial-like Stem Cell Behaviors

A defining feature of embryonic neural development is the acquisition of apico-basal polarity and production of radial glial neural stem cells (Kriegstein and Gotz, 2003). There is evidence that neuroepithelial progenitors in hESC-derived neural rosettes represent apico-basal-like polarity (Elkabetz et al., 2008). When sEBs were plated en-bloc on day 4-7, the adherent EBs (aEBs) flattened and revealed the organization of *NKX2.1*-GFP+ cells in rosette structures. N-cadherin expression was restricted to the rosette luminal surface, confirming polarity, and was consistent with localization to radial glial end feet on the apical ventricular surface in the embryonic brain (Figure 1C). Mitotic marker KI67 was expressed in many cells, particularly in those near the rosette lumen (Figure 1C). In contrast, neuronal markers, ASCL1 (not shown) and DCX (Figure 1C), were detected away from the lumen.

Rosettes were labeled with RFP [*UbiquitinC* promoter-RFP (*UbC*-RFP) virus] and were monitored by live time-lapse imaging. We detected *NKX2.1*-GFP+ and *UbC*-RFP+ cells in rosette structures displaying ventricular zone (VZ) radial glia (vRG)-like interkinetic nuclear migration (INM) behavior prior to division (Figures 1D and 1F). VRG-like cell bodies translocated toward the rosette lumen and divided with a vertical cleavage plane (parallel to the fiber) (Movie S1). Interestingly, daughter cells appeared to extend radial fibers, resembling the symmetrical divisions attributed to embryonic vRGs that divide with a vertical cleavage plane.

We next investigated whether recently described (Fietz et al., 2010; Hansen et al., 2010) human-enriched outer sub-ventricular zone (OSVZ) radial glial (oRG)-like cells were present in our cultures. We focused on *NKX2.1*-GFP+ cells with unipolar fibers located away from the rosette clusters (Figures 1E and 1G). We discovered GFP+ oRG-like cells

displaying mitotic somal translocation (MST) prior to division. These cell bodies translocated toward the unipolar fiber and divided with a horizontal cleavage plane (perpendicular to the fiber) (Movies S2 and S3). In summary, hPSC-derived MGE-like progenitors recapitulated VZ and human-enriched OSVZ radial glial-like stem cell behaviors.

hPSC-derived MGE-like Progenitors Generated GABAergic Interneurons

We further explored the identity and fate of the hPSC-derived MGE-like cultures. Immunostaining analysis was conducted on day 25 aEBs and day 35 dissociated monolayer (ML) cultures, and forebrain marker expression was quantified on day 35 (Figure 2). At both stages, *NKX2.1*-GFP expression was specific to cells expressing endogenous NKX2.1 protein (91.3 ±1.7%). On day 25, FOXG1 and OLIG2 were expressed in most of the *NKX2.1*-GFP+ cells (Figure 2B). By day 35, most GFP+ cells continued to express FOXG1 (81.5 ±3.6%) but had downregulated OLIG2 (6.8 ±3%). Conversely, the majority of GFP+ cells on day 35 upregulated ASCL1 (79.9 ±6.5%) and DLX2 (79.8 ±3.7%) (Figure 2D and 2E). Since OLIG2 marks GE progenitors while ASCL1 and DLX2 mark GABAergic neuronal lineages, these results suggested that MGE-like progenitors began to differentiate into GABAergic neurons and were confirmed by the detection of TUJ1 (92 ±2.4%) and GABA (75.8 ±2.3%) (Figure 2D and 2E). The interneuron subtype marker Calbindin (*CALB1* or CB) was also expressed by day 35 (31.1 ±5.4%), but other interneuron subtype markers Calretinin (*CALB2* or CR), Somatostatin (*SST*), and Parvalbumin (*PVALB* or PV) were not yet detected, suggesting an immature neuronal stage (Figure 2E).

A minority of GFP+ cells expressed NKX2.2 (13.6 ±4.7%), the neural progenitor/glial cell marker GFAP (3.9 ±3.9%), mitotic marker KI67 (2.8 ±1.5%), LGE/POA enriched ISLET1 (7.6 ±3.3%), or dopaminergic neuron marker TH (4.4 ±1.3%). Virtually none of the GFP+ cells expressed PAX6, the CGE/dorsal MGE marker COUPTFII, striatal medium spiny neuron marker DARPP32, globus pallidus projection neuron marker ER81/ETV1, CHAT, or glutamatergic neocortical projection neuron marker TBR1 (Figure 2E). Based on these results, hPSC-derived MGE-like progenitors differentiated into predominantly post-mitotic GABAergic interneuron precursor cells by day 35.

hPSC-derived *NKX2.1*-GFP+ Microarray Profiling

We performed microarray profiling to obtain a global transcriptome comparison of undifferentiated hPSCs and FACS-sorted *NKX2.1*-GFP+ populations over a 55-day time course of differentiation (Figure 3A). The percentage of *NKX2.1*-GFP+ cells remained at a high level in dissociated monolayer culture (~81% on d35) or in co-culture (~94% of RFP+ cells on d55) (Figure 3B). Dendrogram clustering analysis showed the differentiated GFP+ populations to be more closely related to each other than to undifferentiated hPSCs (Figure S4A). We compared transcript expression for panels of lineage-specific markers, and performed quantitative RTPCR to confirm a subset of the array data (Figure 3 and S4B). Markers of pluripotency were only detected in undifferentiated hPSCs, whereas markers of a neuronal lineage (*HES5, TUBB3, DCX, SYP, SYN1*) increased over time in differentiating GFP+ cells. Markers of glial cells, neural crest, or microglia were not detected. We then examined anterior-posterior central nervous system (CNS) patterning and detected expression of primarily anterior CNS markers (*FOXG1, SIX3, OTX2*).

We then investigated markers that identify sub-regions of the forebrain. Aside from temporary expression of *NKX2.2*, markers of diencephalic hypothalamus were not robustly expressed (Figure S4C). Also, dorsal excitatory neuronal lineage markers were not detected (Figure S4D). Instead, ventral telencephalic GABAergic neuronal lineage markers (*ASCL1, DLX1, DLX5*) were expressed along with MGE markers (*NKX2.1, LHX6, LHX8, CXCR7*),

and their expression intensities generally increased over time (Figures 3F and 3H). GABAergic markers (*GAD1, SLC32A1, SLC6A1*) were found, but glutamatergic or cholinergic neuronal markers were not expressed (Figure 3G). Of the interneuron subtype markers, robust *SST* transcript, and weaker *CALB1/2* signals, were detected by day 55 (Figure 3H). These results suggested that GFP+ cells were of a principally telencephalic MGE-like GABAergic interneuron lineage.

Protracted Maturation of hPSC-derived MGE-like Cells into GABAergic Interneurons Expressing Subtype Markers

We sought to determine both the mature neuronal subtypes generated by the *NKX2.1*-GFP+ MGE-like precursors and their developmental timeline. To study their maturation, day 35 FACS-sorted GFP+ cells were co-cultured with cortical glial cells (Figure 4A), and some cells were labeled with *UbC*-RFP virus prior to co-culture. Cultures were fixed for analysis along a time course of 30 weeks post-differentiation (WPD), and interneuron subtype marker expression was quantified. Over time, RFP+ hPSC-derived neurons increased significantly in cell somal size (from 10μm to 30μm by 30 WPD) and displayed more elaborate branching of processes (from 2 to 6 primary branches by 30 WPD) (Figure 4B, n=25 cells or more per time point). Most of the neurons expressed GABA (75-86%) and VGAT (53-78%) from 5-30 WPD (Figure 4C and 4D). Aside from rare cells (11 of 3,110), TBR1 was not expressed.

Similar to cortical interneurons that downregulate NKX2.1 during tangential migration from the MGE to the neocortex (Nobrega-Pereira et al., 2010), the percentage of reporter *NKX2.1*-GFP+ (Figure 4C) and endogenous NKX2.1+ (not shown) neurons significantly declined from five to 30 WPD (96.1 ±1.8% to 66.7 ±6.1%; $p = 0.03$). Conversely, CXCR4 is expressed in migrating cortical interneurons (Wang et al., 2011) and was also upregulated in a fraction (23%) of the hPSC-derived interneurons (Figure 4E), particularly in neurons that downregulated NKX2.1 (47%). LHX6 is a specific marker of the MGE downstream of NKX2.1 and is required for the specification and maturation of SST and PV interneuron subtypes (Zhao et al., 2008). We detected an increasing percentage of hPSC-derived interneurons that expressed LHX6 over time (68 ±3% by 30 WPD). LHX6 was expressed in NKX2.1+ and NKX2.1- neurons (Figure 4E), consistent with its endogenous expression in both MGE-derived cortical and striatal interneuron lineages. Therefore, these results suggest a mixed population of cortical- (NKX2.1-, CXCR4+, LHX6+) and striatal-type (NKX2.1+, CXCR4-, LHX6+) hPSC-MGE-derived interneuron lineages and complement the detection of cortical (*ZEB2 or Zfhx1b, ARX, CXCR4/7*) and striatal (*NKX2.1 and LHX8*) lineage transcripts (Figures 3F and 3H).

We next examined the expression of interneuron subtype markers SST, PV, CB, and CR (Figure 4C and 4D). CB was expressed in neurons throughout the time course (24-36%). In contrast, the percentage of SST+ and CR+ interneurons increased over time and were significantly upregulated from 10 to 20 WPD (SST: 2.8 ±1% to 12.8 ±9%; $p = 0.03$, and CR: 8.8 ±4.9% to 52.6 ±6.2%; $p = 0.004$). By 30 WPD, the percentage of SST+ neurons increased to 40.6 ±8.6%, and CR+ neurons increased to 77.7 ±14.9%. NPY+ neurons were scarce (6 of 819 neurons, not shown). We found neurons expressing PV at 15 WPD (10 ±1.4%, Figure 4F), however only rare PV+ interneurons remained by 30-40 WPD (1.5 ±1.4%). In addition, we did not detect PV lineage marker Kv3.1 (not shown) or fast-spiking firing properties. Since the hPSC-derived interneurons predominantly expressed SST and CR subtype markers, we performed co-staining to determine whether these were distinct or overlapping populations (Figure 4G). We found that only 3.6% of SST+ or CR+ neurons co-expressed these markers by 15 WPD, but 26.3% were co-expressing by 30 WPD. Thus, hPSC-derived interneurons gradually expressed CB, CR, SST, and CR+SST subtype markers along an extensive time course.

Interestingly, this protracted timeline of differentiation appears similar to endogenous human interneuron subtype development (Fertuzinhos et al., 2009). We confirmed these findings with our own histological analysis of developing human fetal and infant cortex and fetal MGE (Figures S5A and S5B). To further investigate human fetal MGE-derived fates, we dissected, labeled with *UbC*-RFP virus, and co-cultured 18 gestational-week (gw) human fetal MGE cells. By 12 weeks in culture, RFP+ human fetal MGE cells had matured into CB +, CR+, SST+, and GABA+ neurons, and they did not express TBR1 (Figure S5C). Therefore, hPSC-derived interneuron maturation paralleled the temporal sequence of endogenous human, and the subtype identities of cultured fetal MGE-derived, interneuron subtype marker expression.

Maturation of hPSC-derived Interneuron Subtype Firing Properties

To test whether the hPSC-derived cells were functional neurons, we performed whole-cell patch recordings to examine their electrophysiological properties at different WPD (8 weeks, n = 21; 12 weeks, n = 35; 15 weeks, n = 31; 30 weeks, n = 18). We found that action potential (AP) firing patterns of hPSC-derived neurons were quite immature at eight WPD, judged by the broad AP 1/2-width of the first AP, small after-hyperpolarization (AHP), reduced AP velocity (dV/dt) in a train of AP firing near threshold, and inability to fire repetitively upon superthreshold current injection (Figures 5C-E and 5I). The peak voltage-gated Na+ and K+ channel currents increased significantly from eight to 12 WPD (Figures 5F and 5G), concomitant with a significant decrease in membrane resistance (Rm) (Figure 5I). Most neurons showed more mature repetitive AP firing upon near threshold current injection at 12 and 15 WPD (Figures 5C, S6B and S6C). By 30 WPD, hPSC-derived neurons exhibited mature AP firing properties with faster and consistent AP velocity near threshold firing (Figure 5C), smaller AP 1/2-width (Figure 5I), and larger AHPs (Figures 5D and 5E), as well as high-frequency repetitive AP firing upon superthreshold current injection (Figures 5C and S6D). We performed post-recording immunostaining analysis on neurobiotin-filled neurons from 30 WPD, and we found 5 out of 7 neurons were SST positive (Figure 5B), consistent with their non-pyramidal regular spiking firing pattern (Figures 5C and S6D).

Along with more mature AP firing properties, we found corresponding changes in the biophysical properties of hPSC-derived interneurons over time. Neurons at 30 WPD showed a significant increase in membrane capacitance (Cm), more hyperpolarized resting membrane potential (RMP), and a significant decrease in membrane resistance (Rm) (Figure 5I) that correlated with increased cell body size and dendritic complexity (Figures 4B and 5A). Consistent with the pace of subtype marker expression, hPSC-derived interneurons demonstrated slow, 30- week maturation of firing properties.

hPSC-derived Interneurons Form Synapses and Generate Functional GABAergic Output

Next, we investigated the synaptic properties of hPSC-derived interneurons co-cultured with mouse glial cells. *NKX2.1*-GFP+ neuronal processes co-localized with punctate pre-synapatic VGAT expression, suggesting the formation of GABAergic synapses (Figure 6A). Spontaneous post-synaptic currents (sPSC) were detected by eight WPD, and the percentage of neurons receiving sPSCs increased from 33.3% at eight WPD (n = 12) to 82.1% at 12 WPD (n = 28), along with increased sPSC frequency (Figures 6C and S6G). Furthermore, sPSCs were fully blocked by the GABAA receptor inhibitor bicuculline methiodide (BMI, 20 μM), indicating functional GABAergic-specific synapse formation (Figure 6B). To confirm that GABAergic neurons were able to send outputs to neighboring neurons, we used optogenetics and transfected half of the cells with *Synapsin* promoter-Channelrhodopsin2-EYFP (ChR2-EYFP). Blue light stimulation reliably induced action potential firing in EYFP-positive neurons (Figure S6F) and evoked robust post-synaptic currents (PSCs) in

neighboring neurons (Figures 6D and 6E). In addition, the PSCs showed a long decay time (31.4 ±1.9 ms, n = 26), characteristic of GABAergic PSCs. This was further verified by reversible blockade of light-evoked PSCs by BMI (Figures 6D and 6E). The reversal potential of light-evoked PSCs was -32.7 mV (Figures 6F and 6G), close to the expected Cl- reversal potential under our recording conditions [-37.3 mV = -53.4 mV (by Nernst equation) + 16.1 mV (junction potential)]. These results demonstrated that the hPSC-derived neurons produced exclusively GABAergic synaptic output.

To examine whether hPSC-derived interneurons could form synapses onto primary human neurons, MGE-like cells were labeled at four WPD with ChR2-YFP and *UbC*-RFP virus, and RFP+ FACS-sorted cells were co-cultured for seven weeks with dissociated human fetal cortical cells from 20gw. Whole-cell recordings were obtained from RFP-negative primary cortical neurons after co-culture (Figure 6H). Blue light stimulation of hPSC-derived neurons induced GABAergic-specific PSCs in recorded primary neurons that were completely blocked by BMI (Figures 6I and 6J). Furthermore, we found polysynaptic responses upon light stimulation (Figure 6I), which were also blocked by BMI, indicating robust GABAergic synaptic integration of hPSC-derived neurons into cultured human fetal neuronal circuits.

hPSC-derived Interneuron Subtype Maturation and Functional Integration in the Mouse Brain

To rigorously evaluate cell fate and function, hPSC-derived MGE-like cells were transplanted into the mouse brain. We modified our protocol to avoid injection of undifferentiated NKX2.1+ neural stem cells and to increase interneuron subtype maturation (See Supplemental Experimental Procedures and Table S2). FACS-sorting purification was used to select for neuronal precursors expressing PSANCAM (Schmandt et al., 2005). An average of 75.7 ±5.2% (n=12) of *NKX2.1*- GFP+ cells were positive for PSA-NCAM expression (Figure S7A). *NKX2.1*-GFP+ and PSA-NCAM+ cells from day 35 ML or day 50 aEB cultures were sorted, some cells labeled with *UbC*-RFP or *Synapsin*-YFP virus, and were injected into severe combined immuno-deficient (SCID) newborn mouse cortex (Figure 7A).

Human cells, detected by staining for human-specific nuclear antigen (HNA), survived for up to seven months post-injection (MPI) (the longest time point) and did not form tumors. Human cell survival rates (% of injected cells) after two, four, and seven MPI were 5.6 ±2.6%, 3.1 ±1.5%, and 8.6 ±3.1%, respectively. By two MPI, human cells expressing HNA and *NKX2.1*-GFP (67.8 ±1.6%), KI67 (25.5 ±1.7%), or DCX (79.8 ±3.8%) were mostly still located near the injection site (Figure S7B). But by three to seven MPI, a fraction of the human cells migrated more than 1mm rostral and caudal into the mouse cortex (Figures 7B and S7C). KI67 and DCX expression were significantly reduced over time (1.7 ±0.27%; $p=0.04$, and 5.9 ±4.9%; $p=0.008$), and *NKX2.1*-GFP was similarly downregulated (35.6 ±14% by 7 MPI). The opposite trend was found for the post-mitotic neuronal marker, NEUN, which increased to 68.4 ±8.3% of human cells by seven MPI (Figure 7C), suggesting the maturation of NKX2.1- and NKX2.1+, cortical- and striatal-like interneurons.

For quantification of subtype maturation, we separated dispersed human cells from those that remained at the injection site. Interestingly, dispersed cells exhibited increased subtype marker expression that also correlated with time post-injection (Figures 7D and 7E), especially for SST. Similar to *in vitro* maturation, dispersed human cells expressed LHX6 (52.7 ±4%), GABA (50.9 ±7%), CB (60.9 ±7%), CR (72.5 ±3%), and SST (50.1 ±6%) by six MPI, and rare PV+ cells were detected. Human cells remaining at the injection site did not robustly express subtype markers, but they appeared to be GABAergic neurons expressing GABA (65.9 ±18%) and NEUN (77.7 ±4%). In summary, hPSC-derived MGE-

like neuronal precursors injected into the mouse brain gradually matured into GABAergic interneuron subtypes.

Lastly, to examine whether hPSC-derived MGE-like cells could develop into functional interneurons that synaptically integrate *in vivo*, we performed whole-cell recordings of RFP + human cells in mouse brain slices seven MPI. Intracellular filling with neurobiotin and post-staining revealed the extensive process branching of recorded RFP+ neurons (Figure 7F). Among 17 total human cells patched from three animals, 16 neurons exhibited the ability to fire action potentials with an average RMP of -64.8 ± 4.0 mV. In addition, two groups of interneurons were identified, type I and type II, with different membrane properties and firing patterns. Type I interneurons had an average RMP of -67.3 ±2.9 mV, Rm of 257 ±78 MΩ, and Cm of 69.4 ±0.6 pF (n=4). The firing pattern of type I interneurons displayed a significant delay to spike at threshold, and little adaptation upon superthreshold, current injection (Figures 7G and S7D). Type II interneurons had more hyperpolarized RMP (-80.1 ±3.4 mV), smaller Rm (91 ±28 MΩ), and smaller Cm (27.7 ±4.6 pF) (n=4). The firing pattern of type II interneurons showed rapid adaptation of initial spikes upon superthreshold current injection (Figures 7G and S7E). Furthermore, the transplanted hPSC-derived interneurons received synaptic inputs (16 of 16) containing both BMI sensitive GABAergic and 6-Cyano-2, 3-dihydroxy-7-nitro-quinoxaline (CNQX) sensitive glutamatergic components (Figure 7H), suggesting functional integration into the host cortex.

DISCUSSION

Here, we model functional human telencephalic-like interneuron subtype maturation from hPSCs and demonstrate their protracted acquisition of mature features. First, we show that hPSC-derived MGE-like progenitors develop through an additional type of radial glial-like stem cell enriched in the human brain. Second, we chronicle the functional maturation of hPSC-derived MGE-like precursors into subtypes of interneurons that slowly develop advanced physiological properties over a prolonged period of time. Third, we find their maturation *in vitro* and post-transplantation parallels the temporal developmental sequence of endogenous human interneurons.

First, MGE-like cells were derived from hPSCs using a robust B27+5F method that harnessed signaling pathways involved in embryonic forebrain development (Rallu et al., 2002; Watanabe et al., 2007). Previously, HES-3 *NKX2.1*$^{GFP/w}$ hESCs were differentiated into hypothalamic forebrain-like precursors in the presence of FGF2 and retinoic acid (RA) (Goulburn et al., 2011). In contrast to this protocol, we detected earlier FOXG1 expression, along with downregulation of NKX2.2 protein, and we did not find RAX expression. Therefore, the B27+5F method favors telencephalic MGE-like differentiation, whereas the FGF2/RA may be useful for diencephalic hypothalamus-like derivation.

An additional type of radial glial stem cell is enriched in the developing human cortical OSVZ, which may contribute to the expanded size of the human brain (Lui et al., 2011). We have also observed these oRG-like cells in the human fetal MGE (unpublished). Here, we used live cell imaging to observe oRG-like, as well as vRG-like, mitotic behaviors in our hPSC-derived MGE-like cultures. In addition to the expansion of neuron numbers, the oRG stem cell stage likely contributes to the extended developmental timeline of human cortical interneurons and pyramidal neurons by delaying their birth. Further study is needed to determine if oRGs are required for the maturation of certain neuronal subtypes.

Second, hPSC-derived MGE-like progenitors matured into mixed cortical- and striatal-like GABAergic interneuron lineages that expressed SST, CR, and CB subtype markers over a 30-week timeline. In association with protracted morphological and subtype marker

maturation, the functional electrophysiological properties of hPSC-derived interneurons also exhibited slow maturation over 30 WPD. Previous work showed that the development of hPSC-derived neuronal firing properties correlated with increasing voltage gated Na^+ and K^+ currents between four and seven WPD (Johnson et al., 2007). Similarly, we found that the amplitude of voltage-gated Na^+ and K^+ currents in our hPSC-derived interneurons increased from eight to 12 WPD. However, mature hPSC-derived interneuron subtype-firing properties were not observed until 30 WPD, despite no further increase in average Na^+ and K^+ currents after 12 WPD, suggesting that the more mature firing properties may result from subtype-specific channel expression (Goldberg et al., 2011). We did not detect the fast-spiking PV+ interneuron subtype by 30 WPD. Since primary PV+ cells are not detected in the cortex until post-natal stages, additional time may be required for their maturation from hPSCs. We observed immature cells that express PV by 15 WPD, however this lineage disappeared at later stages, suggesting that conditions may need to be optimized for their maturation as well. Further methods will also need to be developed in order to preferentially direct the differentiation of either cortical or striatal interneuron lineages or to purify a particular lineage.

Following injection into the mouse brain, hPSC-derived interneuron precursors survived, dispersed from the injection site, matured into subtypes, and functionally integrated into the host cortex. The human cell survival rate was 3-8% of injected cells and is likely an underestimate due to efflux of human cells out of the needle tract at the time of injection. Nevertheless, this rate is not far off from primary mouse fetal MGE cell transplant survival rates of ~10-20%. It is also similar to the 2-10% of mouse ESC-derived MGE-like cells that survived post-injection into the mouse cortex (Maroof et al., 2010). Furthermore, prior reports demonstrated that 1-3% survival of injected primary mouse MGE cells was sufficient for behavioral improvements in rodent models of Parkinson's disease and neuropathic pain (Braz et al., 2012; Martinez-Cerdeno et al., 2010). Thus, the hPSC-derived MGE-like cell survival rate may be sufficient for future cell therapy-based applications.

The human MGE-like cells migrated 1-2mm into the rodent cortex post-injection, similar to mouse ESC-derived MGE-like cells (Maroof et al., 2010). But, they did not migrate as extensively as primary mouse fetal MGE cells, and some cells remained at the injection site. This suggests that optimization of the PSC differentiation stage and/or development of methods to purify migratory MGE-like cells may be needed. Interestingly, the increased expression of interneuron subtype markers correlated with the dispersed fraction of hPSC-derived cells. The interneuron subtypes and protracted timing of marker upregulation post-injection were similar to *in vitro* hPSC maturation. By seven MPI, we identified two groups (type I and II) of hPSC-derived interneurons displaying distinct firing properties. Type I neurons resembled adult mouse delay-spiking (DS) interneurons or non-rebounding regular spiking non-pyramidal cells (NR-RSNPs), which were found to express SST (Butt et al., 2005), and type II neurons were comparable to adult mouse non-fast spiking (NFS1 or NFS2) interneurons that were found to express SST or CR (Miyoshi et al., 2007; Sousa et al., 2009) - consistent with hPSC-derived interneuron subtypes. However, the subtype marker expression profiles of type-I and -II hPSC-derived interneurons remain to be determined.

Despite slow maturation of interneuron subtype-firing properties, we detected GABAergic synaptic activity of hPSC-derived interneurons beginning eight WPD. We used optogenetics to demonstrate robust synaptic integration of hPSC-derived interneurons into cultured primary human neuronal networks. We also detected both GABAergic and glutamatergic synaptic inputs into hPSC-derived interneurons seven MPI into the mouse cortex. Because the hPSC-derived neurons produced GABAergic-exclusive output, glutamatergic synaptic

inputs were likely from host mouse excitatory neurons, indicating that hPSC-interneurons are capable of integrating into host cortical circuits.

Third, the protracted maturation of hPSC-derived interneuron subtype marker expression and firing properties paralleled endogenous human interneuron development. Similar interneuron subtypes were found in the human fetal and infant cortex, and in cultures derived from the human fetal MGE. Moreover, the sequence and timing of subtype marker expression was conserved. These resemblances, and the observation that hPSC-derived interneuron maturation is not accelerated by co-culture or transplantation, suggest interneuron maturation to be an intrinsic program analogous to other MGE interneuron intrinsic programs of plasticity induction and cell death (Southwell et al., 2010; Southwell et al., 2012). In an attempt to estimate neuronal age, we recorded from 22gw human fetal cortical plate neurons and found their AP firing and membrane properties to be considerably immature (Figure 5H and 5I), in agreement with a previous study (Moore et al., 2009), compared to the 30-WPD hPSC-derived interneurons. The hPSC-derived interneurons may represent an early post-natal stage based on similarities to the physiological properties of early-adult non-human primate interneurons (Zaitsev et al., 2009).

In conclusion, we report the stepwise functional maturation of human interneuron subtypes through an hPSC-derived MGE-like intermediate, and we demonstrate the protracted intrinsic development of mature features that model aspects of endogenous post-natal interneurons. Maturation of patient iPSC-derived functional cell types to a post-natal, or more advanced, stage may be critical for creating meaningful disease models, as well as for drug efficacy or toxicity screens. Consistent with this notion, it was reported that hPSC-derived cardiomyocytes only recapitulated adult-onset heart disease phenotypes when adult-stage features had been achieved (Kim et al., 2013). Accordingly, hPSC-derived SST+ interneuron subtypes, which required 20-30 WPD for functional maturation, may be affected in adult temporal lobe epilepsy (TLE) (de Lanerolle et al., 2003; Robbins et al., 1991) and may provide a substrate to identify drugs that enhance their function. Our findings also provide a framework for future patient iPSC modeling of diseases linked to interneuron dysfunction. However, since many diseases are adult onset, hPSC-derived interneurons may need to be matured even further to be useful. Based on their remarkably lengthy timeline, it will be interesting to study the mechanisms regulating human interneuron maturation and to possibly uncover means to accelerate their development. Discoveries along these lines would facilitate hPSC-based regenerative medicine applications.

EXPERIMENTAL PROCEDURES

Cell Culture

HES-3 hESCs were maintained on irradiated mouse embryonic fibroblasts (Millipore) in knockout DMEM with 20% knockout serum replacement, 1% non-essential amino acids (NEAA), 1% pen-strep-glutamine, 0.0008% 2-mercaptoethanol, and 10 ng/mL FGF-basic (Invitrogen). Differentiation was initiated by CollagenaseIV/Dispase (1mg/mL each; Invitrogen) preferential selection for hESC colonies. Colonies were trypsinized to single cells, and, as described (Eiraku et al., 2008), ~10,000 cells/well were plated into low-attachment round-bottom 96-well plates (Corning or NOF) to form one sEB/well in optimized B27+5F differentiation medium #1, consisting of Neurobasal-A, 2% B27-vitamin A (Invitrogen), and the same supplements in hESC media but without FGF. Also, Y27632 (10μM), SB431542 (10μM), Purmorphamine (1-2 μM) (Stemgent), BMPRIA-Fc (1.5μg/mL), and DKK1 (1μg/mL) (Invitrogen) were added. See Supplemental Experimental Procedures for more information. All experiments conducted on hESCs and human fetal tissue adhered to approved UCSF Stem Cell Research Oversight committee and Committee on Human Research protocols.

Transplantation

Excess medium was removed from sorted cell pellets to create concentrated cell suspensions of 1000cells/nl. Cells were loaded into a beveled glass micropipette (Wiretrol 5ul, Drummond Scientific Company) mounted on a stereotactic hydraulic injector. P2 CB.17-SCID pups (Charles River) were anesthetized through hypothermia and positioned in a clay head mold on the injector platform. 10-100,000cells per injection site were delivered transcranially into the right cerebral cortex using the following coordinates: 0.9mm from the midline (sagittal sinus), and 2.6mm from lambda. The depth of injection was 0.45mm from the skin surface. All transplantation experiments adhered to approved UCSF Institutional Animal Care and Use Committee protocols.

Immunostaining

Cultured cells were fixed in 4% paraformaldehyde for 10-20min. Mouse brains were fixed overnight-4°C after trans-cardial perfusion and sectioned (50μm) by vibratome or sliding microtome. EBs and human tissue were sectioned (25 μm) by cryostat. Cells and sections were stained: 5-10min antigen retrieval with boiling 0.01M citrate buffer pH=6, 1hr block with 5% serum and 0.1% tritonX100 in PBS, overnight-4°C primary antibody in block buffer (except triton-free buffer used for GABA antibody), wash 3× in PBS+tritonX100, 2hr secondary antibody (Invitrogen), wash 4× in PBS+tritonX100. Primary antibodies are listed in Table S3.

Transcript Expression

RNA was prepared from cell pellets with RNEasy kit (Qiagen). CDNA was prepared with Superscript III-first strand kit (Invitrogen). Quantitative RTPCR was performed with SYBR green master mix on a real-time PCR system (Applied Biosystems). Reverse-transcriptase negative controls were used. Amplicon specificity was determined by gel-electrophoresis and melt-curve analysis. Primer sequences are listed in Table S3.

For microarray analysis, RNA was submitted to the Southern California Genotyping Consortium for hybridization to Illumina Human HT-12 v4.0 expression bead-chip. hESC = one sample and four technical replicates. D20 = three independent samples. D35 = one sample and two technical replicates. D55 = one sample and one technical replicate. Data was analyzed with GenomeStudio (Illumina) software. Probes without signal were validated by confirming hybridization to control human brain reference RNA and/or to samples archived in ArrayExpress. Data was deposited in the Gene Expression Omnibus (GEO).

Electrophysiology and Optical Methods

The patch electrodes were made from borosilicate glass capillaries (B-120-69-15, Sutter Instruments) with a resistance in the range of 5-7 MΩ. The pipettes were tip-filled with internal solution containing (in mM): 125 K-gluconate, 15 KCl, 10 HEPES, 4 MgCl2, 4 Na2ATP, 0.3 Na3GTP, 10 Tris-phosphocreatine, 0.2 EGTA. See Supplemental Experimental Procedures for more information.

Statistical Analyses

Data are presented as mean ± s.e.m. Figure 2E data are represented as mean % of co-expressing/GFP+ cells. Figure 3C-H data as mean bead signal intensity. Figure 4C data as mean % of UbC-RFP+, ChR2-YFP+, or TUJ+ neurons. Figure 7C-D data as mean % of HNA+ or UbC-RFP+ human cells. Statistical comparisons used one-way ANOVA with *post hoc* Bonferroni test for electrophysiology data, and used a two-tailed, two-sample unequal variance Student's t-Test for immunostaining data. Cell counts were calculated with Imaris

(Bitplane) software using MATLAB plugin. A summary of sample sizes and cell counts for each experiment and marker are listed in Table S4.

Supplementary Material

Refer to Web version on PubMed Central for supplementary material.

Acknowledgments

We thank Scott Baraban, Robert Hunt, Doris Wang, Stephen Gee, Philip Parker, and Mingpo Yang for electrophysiology guidance and discussion. We thank David Hansen, Jan Lui, Michael Oldham, Mercedes Paredes, Corey Harwell, Xiaoqun Wang, Shaohui Wang, Yingying Wang, Sophia Hart, Ricardo Romero, Thuhien Nguyen, and William Walantus for helpful discussion, gene expression, cell culture, tissue procurement, processing, and technical assistance. We thank Kenneth Probst for graphical design. We thank Miguel Ramalho-Santos and Yuki Ohi for hiPSC lines, Karl Deisseroth for the ChR2-EYFP plasmid, and Kazuaki Yoshikawa for the DLX2 antibody. We thank the staff and faculty at San Francisco General Hospital Women's Options Center and at Advanced Bioscience Resources, who assisted in human fetal tissue collection. This work was supported by the California Institute of Regenerative Medicine (RC1-00346 to ARK; RB2-01602 to JLR; TR2-01749 to AAB) and the Osher Foundation. JC is a recipient of the CARE & CURE Pediatric Epilepsy Fellowship from Epilepsy Foundation of Greater Los Angeles. AGE and EGS are Senior Research Fellows of the NHMRC of Australia. CRN, AAB, JLR, and ARK are board members and shareholders of Neurona Therapeutics.

References

Anderson SA, Marin O, Horn C, Jennings K, Rubenstein JL. Distinct cortical migrations from the medial and lateral ganglionic eminences. Development. 2001; 128:353–363. [PubMed: 11152634]

Braz JM, Sharif-Naeini R, Vogt D, Kriegstein A, Alvarez-Buylla A, Rubenstein JL, Basbaum AI. Forebrain GABAergic neuron precursors integrate into adult spinal cord and reduce injury-induced neuropathic pain. Neuron. 2012; 74:663–675. [PubMed: 22632725]

Butt SJ, Fuccillo M, Nery S, Noctor S, Kriegstein A, Corbin JG, Fishell G. The temporal and spatial origins of cortical interneurons predict their physiological subtype. Neuron. 2005; 48:591–604. [PubMed: 16301176]

Chambers SM, Fasano CA, Papapetrou EP, Tomishima M, Sadelain M, Studer L. Highly efficient neural conversion of human ES and iPS cells by dual inhibition of SMAD signaling. Nat Biotechnol. 2009; 27:275–280. [PubMed: 19252484]

Chao HT, Chen H, Samaco RC, Xue M, Chahrour M, Yoo J, Neul JL, Gong S, Lu HC, Heintz N, et al. Dysfunction in GABA signalling mediates autism-like stereotypies and Rett syndrome phenotypes. Nature. 2010; 468:263–269. [PubMed: 21068835]

Cheah CS, Yu FH, Westenbroek RE, Kalume FK, Oakley JC, Potter GB, Rubenstein JL, Catterall WA. Specific deletion of NaV1.1 sodium channels in inhibitory interneurons causes seizures and premature death in a mouse model of Dravet syndrome. Proc Natl Acad Sci U S A. 2012; 109:14646–14651. [PubMed: 22908258]

Cobos I, Calcagnotto ME, Vilaythong AJ, Thwin MT, Noebels JL, Baraban SC, Rubenstein JL. Mice lacking Dlx1 show subtype-specific loss of interneurons, reduced inhibition and epilepsy. Nat Neurosci. 2005; 8:1059–1068. [PubMed: 16007083]

de Lanerolle NC, Kim JH, Williamson A, Spencer SS, Zaveri HP, Eid T, Spencer DD. A retrospective analysis of hippocampal pathology in human temporal lobe epilepsy: evidence for distinctive patient subcategories. Epilepsia. 2003; 44:677–687. [PubMed: 12752467]

Eiraku M, Watanabe K, Matsuo-Takasaki M, Kawada M, Yonemura S, Matsumura M, Wataya T, Nishiyama A, Muguruma K, Sasai Y. Self-organized formation of polarized cortical tissues from ESCs and its active manipulation by extrinsic signals. Cell Stem Cell. 2008; 3:519–532. [PubMed: 18983967]

Elkabetz Y, Panagiotakos G, Al Shamy G, Socci ND, Tabar V, Studer L. Human ES cell-derived neural rosettes reveal a functionally distinct early neural stem cell stage. Genes Dev. 2008; 22:152–165. [PubMed: 18198334]

Espuny-Camacho I, Michelsen KA, Gall D, Linaro D, Hasche A, Bonnefont J, Bali C, Orduz D, Bilheu A, Herpoel A, et al. Pyramidal neurons derived from human pluripotent stem cells integrate efficiently into mouse brain circuits in vivo. Neuron. 2013; 77:440–456. [PubMed: 23395372]

Fazzari P, Paternain AV, Valiente M, Pla R, Lujan R, Lloyd K, Lerma J, Marin O, Rico B. Control of cortical GABA circuitry development by Nrg1 and ErbB4 signalling. Nature. 2010; 464:1376–1380. [PubMed: 20393464]

Fertuzinhos S, Krsnik Z, Kawasawa YI, Rasin MR, Kwan KY, Chen JG, Judas M, Hayashi M, Sestan N. Selective depletion of molecularly defined cortical interneurons in human holoprosencephaly with severe striatal hypoplasia. Cereb Cortex. 2009; 19:2196–2207. [PubMed: 19234067]

Fietz SA, Kelava I, Vogt J, Wilsch-Brauninger M, Stenzel D, Fish JL, Corbeil D, Riehn A, Distler W, Nitsch R, et al. OSVZ progenitors of human and ferret neocortex are epithelial-like and expand by integrin signaling. Nat Neurosci. 2010; 13:690–699. [PubMed: 20436478]

Goldberg EM, Jeong HY, Kruglikov I, Tremblay R, Lazarenko RM, Rudy B. Rapid developmental maturation of neocortical FS cell intrinsic excitability. Cereb Cortex. 2011; 21:666–682. [PubMed: 20705896]

Goulburn AL, Alden D, Davis RP, Micallef SJ, Ng ES, Yu QC, Lim SM, Soh CL, Elliott DA, Hatzistavrou T, et al. A targeted NKX2.1 human embryonic stem cell reporter line enables identification of human basal forebrain derivatives. Stem Cells. 2011; 29:462–473. [PubMed: 21425409]

Hansen DV, Lui JH, Parker PR, Kriegstein AR. Neurogenic radial glia in the outer subventricular zone of human neocortex. Nature. 2010; 464:554–561. [PubMed: 20154730]

Johnson MA, Weick JP, Pearce RA, Zhang SC. Functional neural development from human embryonic stem cells: accelerated synaptic activity via astrocyte coculture. J Neurosci. 2007; 27:3069–3077. [PubMed: 17376968]

Kim C, Wong J, Wen J, Wang S, Wang C, Spiering S, Kan NG, Forcales S, Puri PL, Leone TC, et al. Studying arrhythmogenic right ventricular dysplasia with patient-specific iPSCs. Nature. 2013

Kim JE, O'Sullivan ML, Sanchez CA, Hwang M, Israel MA, Brennand K, Deerinck TJ, Goldstein LS, Gage FH, Ellisman MH, et al. Investigating synapse formation and function using human pluripotent stem cell-derived neurons. Proc Natl Acad Sci U S A. 2011; 108:3005–3010. [PubMed: 21278334]

Kriegstein AR, Gotz M. Radial glia diversity: a matter of cell fate. Glia. 2003; 43:37–43. [PubMed: 12761864]

Le Magueresse C, Monyer H. GABAergic interneurons shape the functional maturation of the cortex. Neuron. 2013; 77:388–405. [PubMed: 23395369]

Li XJ, Zhang X, Johnson MA, Wang ZB, Lavaute T, Zhang SC. Coordination of sonic hedgehog and Wnt signaling determines ventral and dorsal telencephalic neuron types from human embryonic stem cells. Development. 2009; 136:4055–4063. [PubMed: 19906872]

Lui JH, Hansen DV, Kriegstein AR. Development and evolution of the human neocortex. Cell. 2011; 146:18–36. [PubMed: 21729779]

Ma L, Hu B, Liu Y, Vermilyea SC, Liu H, Gao L, Sun Y, Zhang X, Zhang SC. Human embryonic stem cell-derived GABA neurons correct locomotion deficits in quinolinic acid-lesioned mice. Cell Stem Cell. 2012; 10:455–464. [PubMed: 22424902]

Markram H, Toledo-Rodriguez M, Wang Y, Gupta A, Silberberg G, Wu C. Interneurons of the neocortical inhibitory system. Nat Rev Neurosci. 2004; 5:793–807. [PubMed: 15378039]

Maroof AM, Brown K, Shi SH, Studer L, Anderson SA. Prospective isolation of cortical interneuron precursors from mouse embryonic stem cells. J Neurosci. 2010; 30:4667–4675. [PubMed: 20357117]

Martinez-Cerdeno V, Noctor SC, Espinosa A, Ariza J, Parker P, Orasji S, Daadi MM, Bankiewicz K, Alvarez-Buylla A, Kriegstein AR. Embryonic MGE precursor cells grafted into adult rat striatum integrate and ameliorate motor symptoms in 6-OHDA-lesioned rats. Cell Stem Cell. 2010; 6:238–250. [PubMed: 20207227]

Miyoshi G, Butt SJ, Takebayashi H, Fishell G. Physiologically distinct temporal cohorts of cortical interneurons arise from telencephalic Olig2-expressing precursors. J Neurosci. 2007; 27:7786–7798. [PubMed: 17634372]

Moore AR, Filipovic R, Mo Z, Rasband MN, Zecevic N, Antic SD. Electrical excitability of early neurons in the human cerebral cortex during the second trimester of gestation. Cereb Cortex. 2009; 19:1795–1805. [PubMed: 19015375]

Nobrega-Pereira S, Gelman D, Bartolini G, Pla R, Pierani A, Marin O. Origin and molecular specification of globus pallidus neurons. J Neurosci. 2010; 30:2824–2834. [PubMed: 20181580]

Rallu M, Corbin JG, Fishell G. Parsing the prosencephalon. Nat Rev Neurosci. 2002; 3:943–951. [PubMed: 12461551]

Robbins RJ, Brines ML, Kim JH, Adrian T, de Lanerolle N, Welsh S, Spencer DD. A selective loss of somatostatin in the hippocampus of patients with temporal lobe epilepsy. Ann Neurol. 1991; 29:325–332. [PubMed: 1675046]

Schmandt T, Meents E, Gossrau G, Gornik V, Okabe S, Brustle O. High-purity lineage selection of embryonic stem cell-derived neurons. Stem Cells Dev. 2005; 14:55–64. [PubMed: 15725744]

Shi Y, Kirwan P, Smith J, Robinson HP, Livesey FJ. Human cerebral cortex development from pluripotent stem cells to functional excitatory synapses. Nat Neurosci. 2012; 15:477–486. S471. [PubMed: 22306606]

Shimamura K, Rubenstein JL. Inductive interactions direct early regionalization of the mouse forebrain. Development. 1997; 124:2709–2718. [PubMed: 9226442]

Sousa VH, Miyoshi G, Hjerling-Leffler J, Karayannis T, Fishell G. Characterization of Nkx6-2-derived neocortical interneuron lineages. Cereb Cortex. 2009; 19(Suppl 1):i1–10. [PubMed: 19363146]

Southwell DG, Froemke RC, Alvarez-Buylla A, Stryker MP, Gandhi SP. Cortical plasticity induced by inhibitory neuron transplantation. Science. 2010; 327:1145–1148. [PubMed: 20185728]

Southwell DG, Paredes MF, Galvao RP, Jones DL, Froemke RC, Sebe JY, Alfaro-Cervello C, Tang Y, Garcia-Verdugo JM, Rubenstein JL, et al. Intrinsically determined cell death of developing cortical interneurons. Nature. 2012; 491:109–113. [PubMed: 23041929]

Verret L, Mann EO, Hang GB, Barth AM, Cobos I, Ho K, Devidze N, Masliah E, Kreitzer AC, Mody I, et al. Inhibitory interneuron deficit links altered network activity and cognitive dysfunction in Alzheimer model. Cell. 2012; 149:708–721. [PubMed: 22541439]

Wang Y, Li G, Stanco A, Long JE, Crawford D, Potter GB, Pleasure SJ, Behrens T, Rubenstein JL. CXCR4 and CXCR7 have distinct functions in regulating interneuron migration. Neuron. 2011; 69:61–76. [PubMed: 21220099]

Watanabe K, Ueno M, Kamiya D, Nishiyama A, Matsumura M, Wataya T, Takahashi JB, Nishikawa S, Muguruma K, Sasai Y. A ROCK inhibitor permits survival of dissociated human embryonic stem cells. Nat Biotechnol. 2007; 25:681–686. [PubMed: 17529971]

Wichterle H, Turnbull DH, Nery S, Fishell G, Alvarez-Buylla A. In utero fate mapping reveals distinct migratory pathways and fates of neurons born in the mammalian basal forebrain. Development. 2001; 128:3759–3771. [PubMed: 11585802]

Zaitsev AV, Povysheva NV, Gonzalez-Burgos G, Rotaru D, Fish KN, Krimer LS, Lewis DA. Interneuron diversity in layers 2-3 of monkey prefrontal cortex. Cereb Cortex. 2009; 19:1597–1615. [PubMed: 19015370]

Zhao Y, Flandin P, Long JE, Cuesta MD, Westphal H, Rubenstein JL. Distinct molecular pathways for development of telencephalic interneuron subtypes revealed through analysis of Lhx6 mutants. J Comp Neurol. 2008; 510:79–99. [PubMed: 18613121]

HIGHLIGHTS

- hPSC-derived MGE-like GABAergic interneurons model human neural development
- MGE-like progenitors display human-enriched radial glial stem cell complexity
- MGE-like cells exhibit protracted maturation into functional interneuron subtypes
- MGE-like cells mature and functionally integrate post-injection in the mouse brain

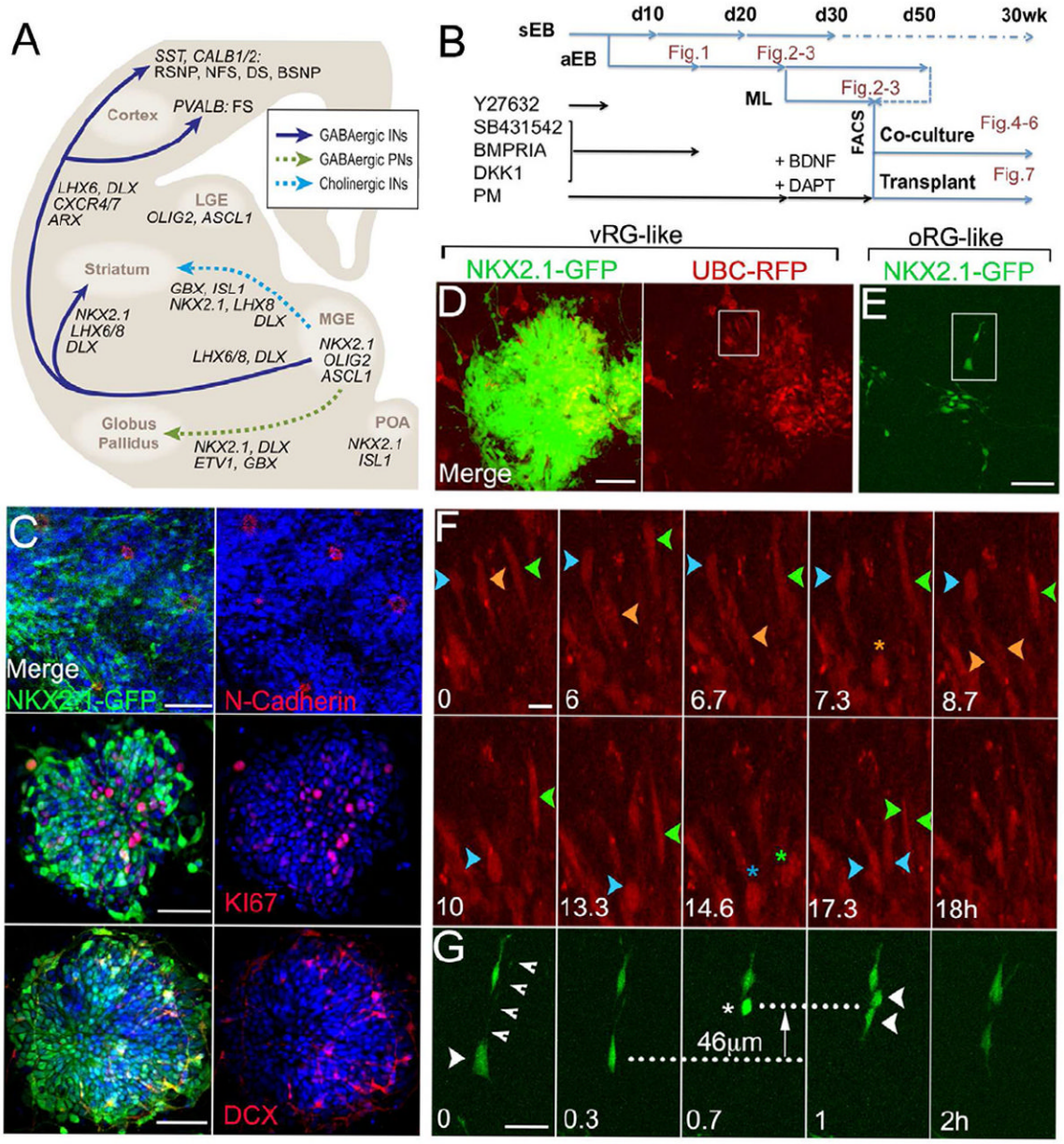

Figure 1. hPSC-derived MGE-like Progenitors Exhibited VZ and SVZ Radial Glial-like Stem Cell Divisions

(A) Schematic of neuronal lineages emanating from the MGE, their gene expression profiles, and major cortical interneuron subtypes. Abbreviations: INs – Interneurons, PNs – Projection Neurons, FS – Fast Spiking, RSNP – Regular Spiking Non-Pyramidal, NFS – Non-Fast Spiking, DS – Delayed Spiking, BSNP – Burst Spiking Non-Pyramidal.

(B) Outline of B27+5F method and corresponding figures. Abbreviations: sEB= suspension embryoid body; aEB= adherent embryoid body; ML= monolayer; FACS= fluorescence activated cell sorting; Y27632= Rho-associated kinase (ROCK) inhibitor; SB431542= inhibitor of the TGFβ1 activin receptor-like kinases; BMPRIA= Bone Morphogenetic Protein Receptor 1a Fc chimera; DKK1= Dickkopf homolog 1; PM= Purmorphamine; BDNF= Brain-derived Neurotrophic Factor; DAPT= inhibitor of γ-secretase. See also Supplemental Experimental Procedures, Figures S1-3, and Table S1.

(C) Day 14 *NKX2.1*-GFP expression and a panel of markers in red shown merged and separate: N-Cadherin, KI67, and DCX. Blue: DAPI. Scale Bar: 50 μm.
(D) A cluster of rosettes with RFP fluorescence alone or merged with *NKX2.1*-GFP.
(E) *NKX2.1*-GFP expressing cells outside of the clusters. D,E Scale Bar: 100 μm.
(F) Time-lapse imaging series of boxed region (D) showing three RFP+ cells (blue, orange, and green arrowheads) that displayed vRG-like INM behavior: translocation toward the rosette lumen and division (star) with a vertical cleavage plane. Time: hours. Scale Bar: 20 μm. See also Movie S1.
(G) Time-lapse series of boxed region (E). A GFP+ cell with characteristic unipolar morphology (white arrowhead and smaller arrowheads to mark fiber) exhibited oRG-like MST behavior: translocation toward the fiber (46μm) and division (star) with a horizontal cleavage plane. Time: hours. Scale Bar: 50 μm. See also Movies S2 and S3.

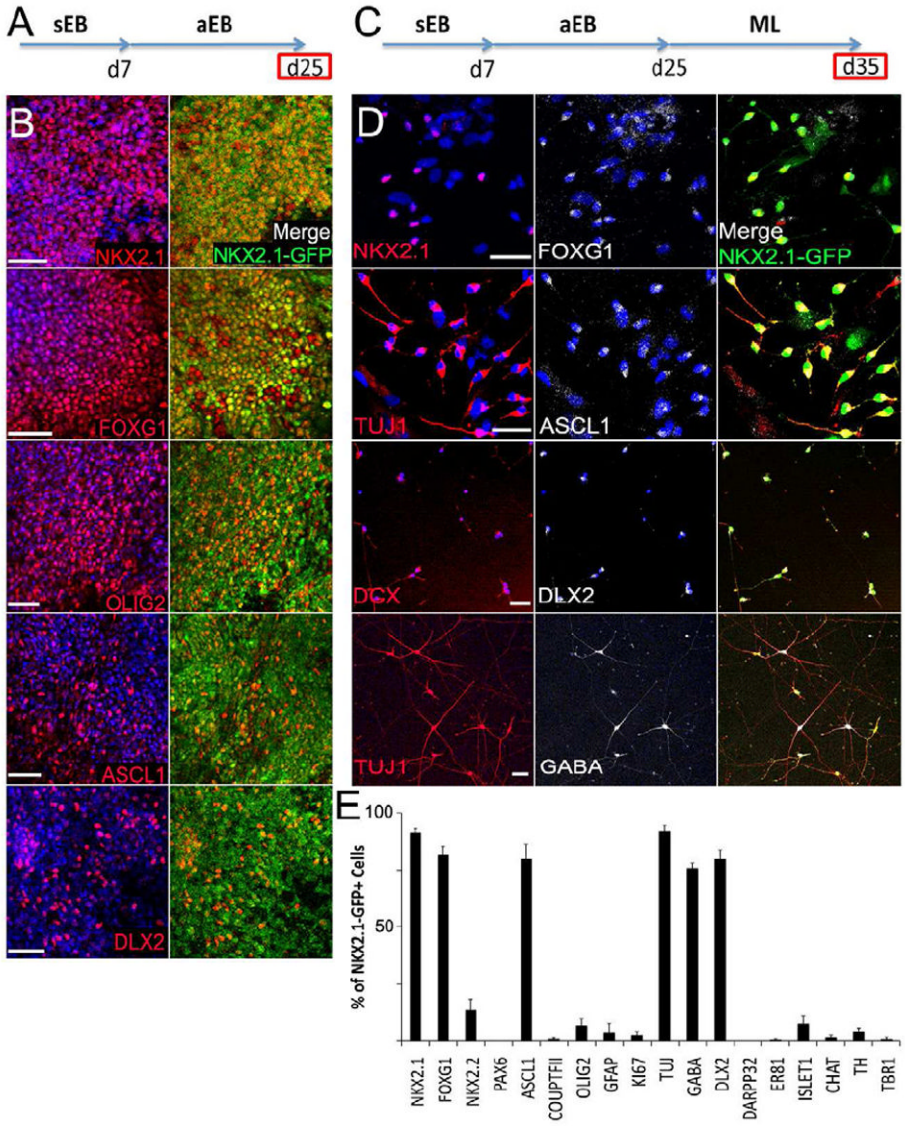

Figure 2. hPSC-derived MGE-like Progenitors Differentiated into Neurons with Properties of Telencephalic GABAergic Interneurons

(A) aEBs fixed for immunofluorescence analysis on day 25.

(B) Day 25 MGE-like progenitor cells robustly expressed *NKX2.1*-GFP, NKX2.1, FOXG1, and OLIG2. Some expressed ASCL1 and DLX2. Blue: DAPI. Scale Bar: 50 μm.

(C) aEBs dissociated, replated as a ML, and fixed for day 35 immunofluorescence.

(D) Day 35 dissociated cells continued to express *NKX2.1*-GFP, NKX2.1, and FOXG1, and upregulated TUJ1, ASCL1, DCX, DLX2, and GABA. Blue: DAPI. Scale Bar: 50 μm.

(E) Quantification of day 35 immunostaining. The majority of *NKX2.1*-GFP+ cells expressed NKX2.1, FOXG1, ASCL1, TUJ, GABA, and DLX2. Data represented as mean ± SEM.

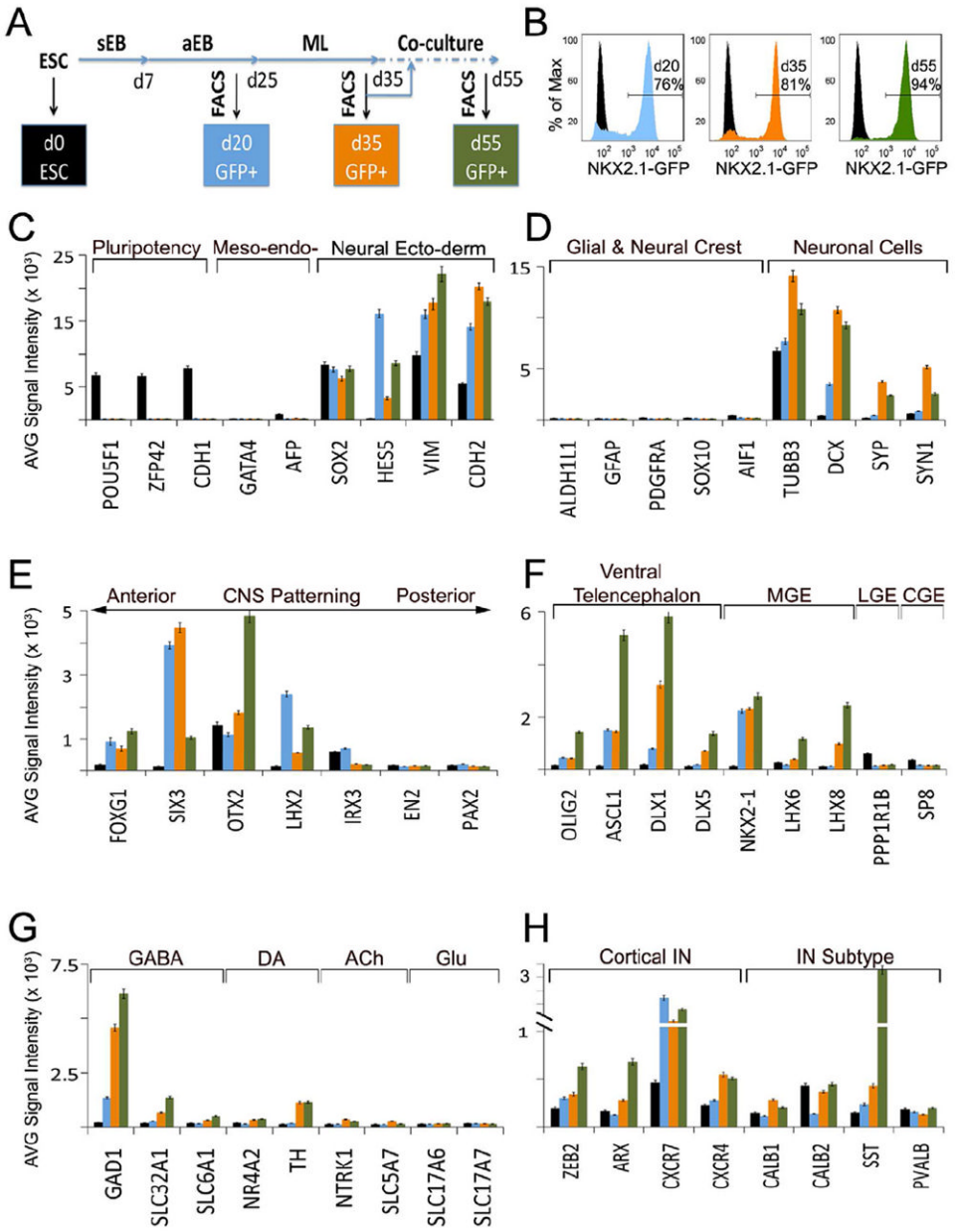

Figure 3. Microarray Gene Expression Profiling of hPSC-derived MGE-like *NKX2.1*-GFP+ Cell Populations

(A) Schematic and legend for microarray data. Undifferentiated hPSCs (black); and FACS-sorted GFP+ cells from day 20 aEBs (blue), day 35 ML cultures (orange), and GFP+ cells from d35 co-cultured to day 55 (green).

(B) Representative FACS histogram analysis of each differentiation stage and undifferentiated hPSC controls (black).

(C-H) Average transcript hybridization signal intensities for marker panels. IN=interneuron, DA=dopaminergic, ACh=cholinergic, Glu=glutamatergic. Data represented as mean ± SEM. See also Figure S4.

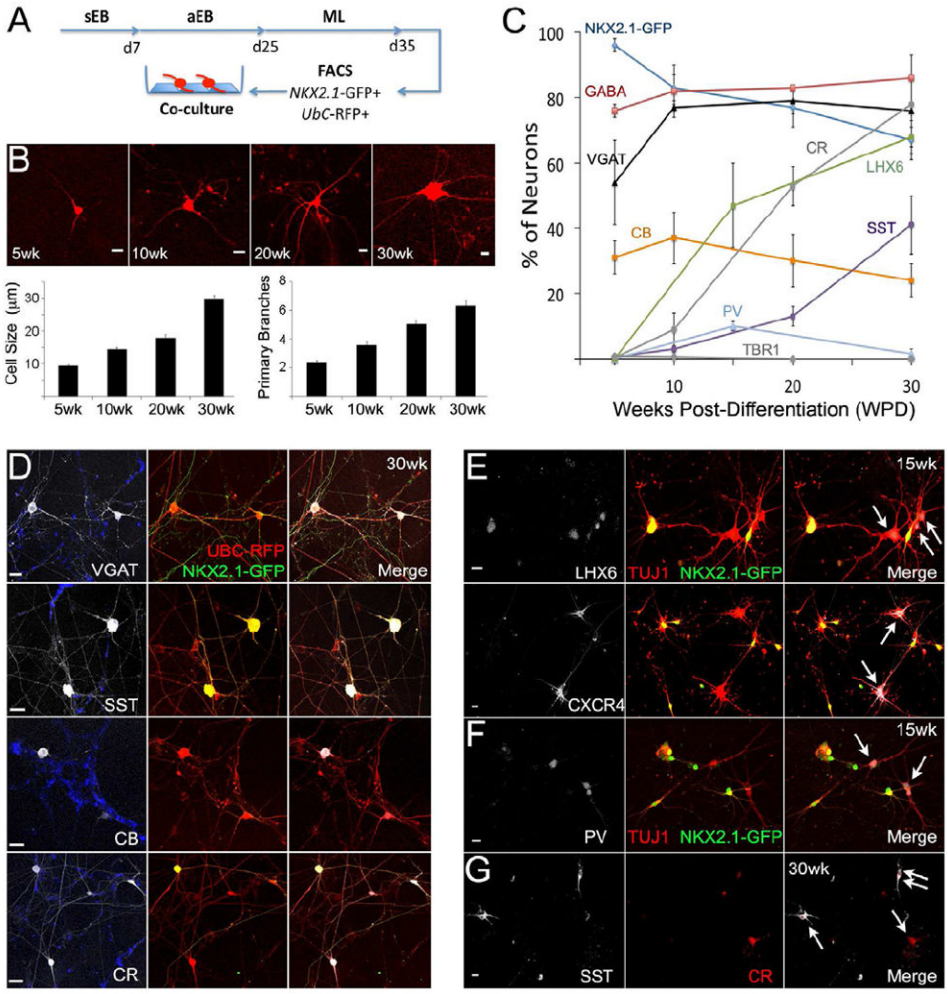

Figure 4. Maturation of hPSC-derived GABAergic Interneurons Expressing Subtype Markers

(A) Dissociated ML cultures infected with *UbC*-RFP lentivirus, FACS-sorted on day 35 for GFP+ and RFP+ cells, and co-cultured.

(B) RFP+ neurons increased in size and dendritic complexity over time. Scale Bar: 20 μm. Cell somal size (μm) and # of primary branches quantified as mean ± SEM.

(C) Quantification of immunostaining analyses over 30 WPD. Data represented as mean ± SEM.

(D) Immunostaining of 30 WPD cultures showing highly branched RFP+ neurons that expressed VGAT, SST, CALB, and CALR. Scale Bar: 50 μm.

(E-F) hPSC-derived TUJ1+ neurons at 15 WPD expressed LHX6, CXCR4, and PV. Some LHX6+, and most CXCR4+ and PV+, neurons downregulated NKX2.1 (arrows), suggesting a cortical-type interneuron lineage.

(G) Double immunolabeling for SST and CR at 30 WPD. Single positives (arrows) and double positive (double arrows). E-G Scale Bars: 20 μm. See also Figure S5.

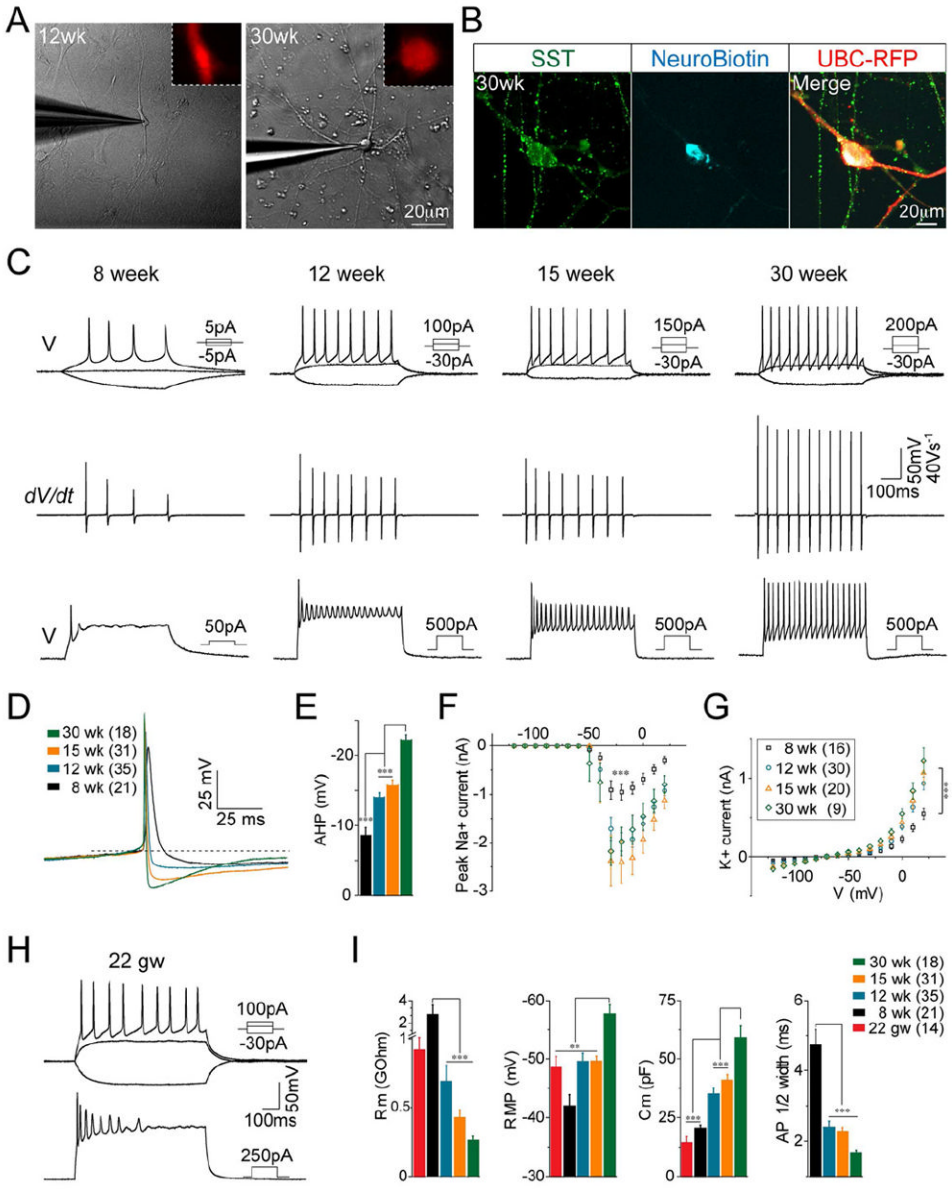

Figure 5. Maturation of hPSC-derived Interneuron Firing Properties

(A) DIC image of hPSC-derived neurons at 12 and 30 WPD, insets show RFP expression of recorded neurons.

(B) hPSC-derived neuron labeled by intracellular filling with neurobiotin immunostained positive for SST at 30 WPD

(C) Representative AP firing patterns at each stage upon near threshold (top) and superthreshold (bottom) current injection, and AP velocity (dV/dt) at threshold firing (middle). Scale bars: 50 mV or 40 Vs^{-1} for dV/dt, 100 ms. See also Figure S6.

(D) Average first AP traces upon threshold current injection. Scale bars: 25 mV and 25 ms.

(E) Statistical results showing AHPs at each stage (dashed line=baseline).

(F) I-V curve of Na^+ (I) and K^+ currents (G) at each stage, measured under stepped voltages (500 ms duration).

(H) Representative AP firing patterns of 22 gestational week (gw) human fetal cortical neurons upon near threshold (upper) and superthreshold (lower) current injection. Scale bars 50 mV and 100 ms.
(I) Statistical results showing membrane resistance (Rm), resting membrane potential (RMP), membrane capacitance (Cm), and action potential (AP) 1/2-width. E, F, G, I: Data represented as mean ± SEM. ** represents $p < 0.01$, *** represents $p < 0.001$.

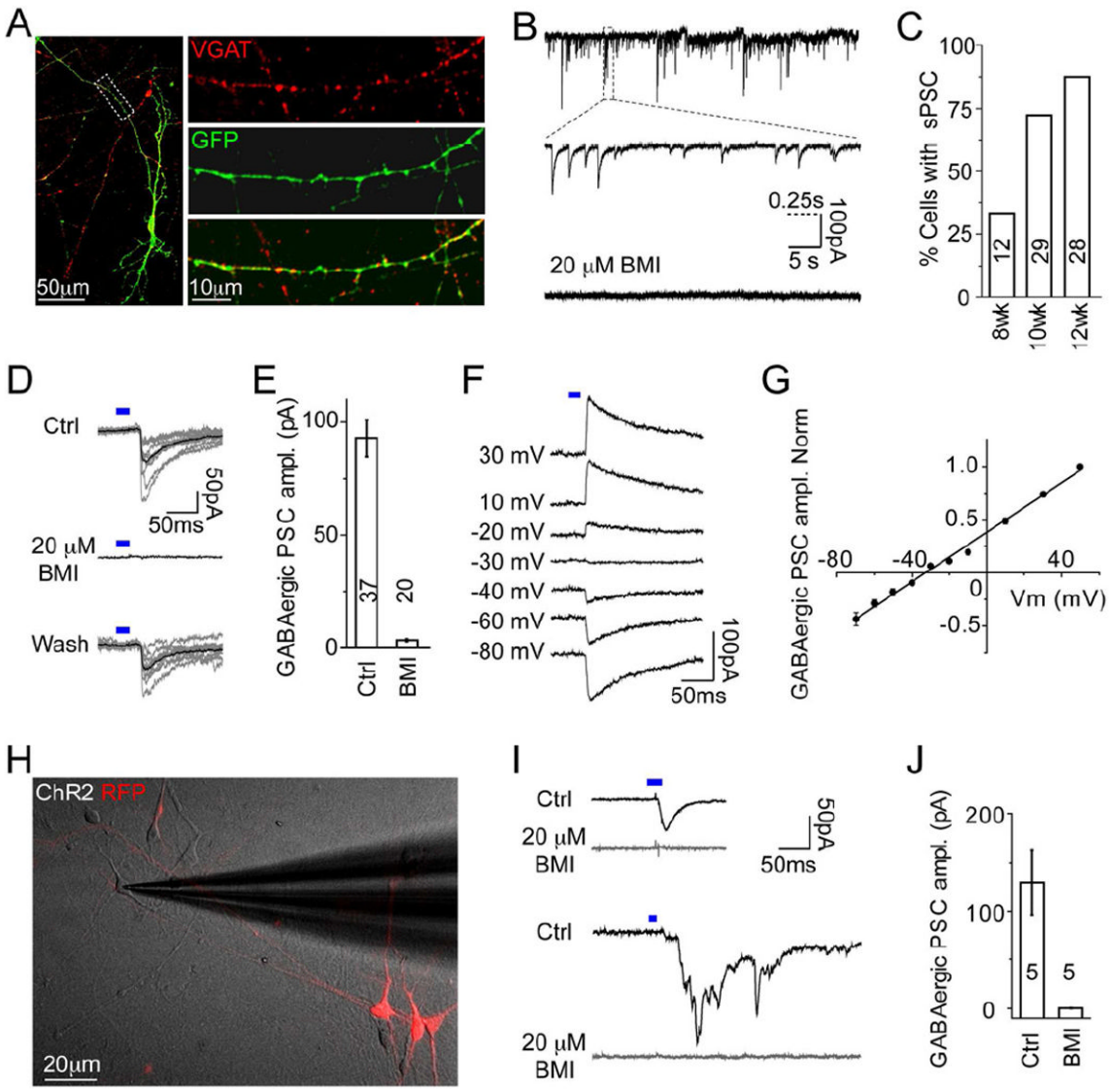

Figure 6. Functional GABAergic Synaptic Properties of hPSC-derived Interneurons

(A) Images showing VGAT expression in hPSC-derived *NKX2.1*-GFP+ neurons at 12 WPD. Right: zoom of dashed rectangle. Scale bar: left, 50 μm; right, 10 μm.

(B) Traces showing spontaneous post-synaptic currents (PSCs) in hPSC-derived neurons, bottom: PSCs were fully blocked by BMI. Scale bar: 100 pA, 5 s and 0.25 s (dashed line) for middle trace.

(C) Percentage of neurons showing spontaneous PSCs at different stages.

(D) hPSC-derived neurons were transfected with ChR2-EYFP. Traces show pulses of blue light (blue bar) evoked PSCs in neighboring cells that were reversibly blocked by BMI. Scale bar: 50 pA and 50 ms. See also Figure S6.

(E) Average amplitudes of light-evoked GABAergic PSCs and application of BMI.

(F-G) Traces showing light-evoked (blue bar) PSCs at different holding potentials. Summarized results (n=7) showing I-V curve of light-evoked GABAergic PSCs (G).

(H) Merged image showing DIC of human fetal cortical cells co-cultured with sorted *UbC*-RFP+ and ChR2 transfected hPSC-derived neurons. Scale bar: 20 μm.

(I) Traces showing blue light (blue bar) stimulation of hPSC-derived neuron-evoked PSCs in RFP-negative recorded human fetal cortical neurons. Upper panel shows PSC mono-synaptic response, lower panel shows PSC with poly-synaptic responses – both fully blocked by BMI. Scale bar: 50pA and 50 ms.
(J) Averaged amplitudes of light-evoked PSCs and application of BMI.
E, J: Data represented as mean ± SEM.

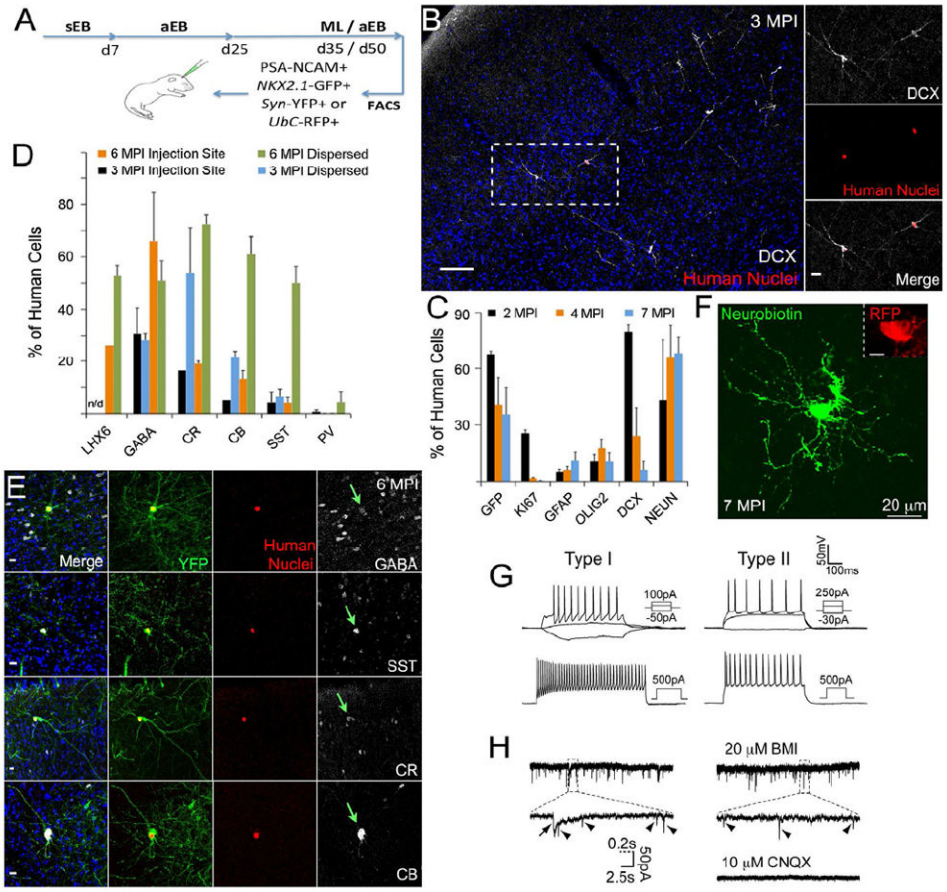

Figure 7. hPSC-derived Interneuron Subtype Maturation and Functional Integration in the Mouse Brain

(A) hPSC-derived MGE-like interneuron precursors FACS-sorted for *NKX2.1*-GFP and PSA-NCAM, labeled with YFP or RFP virus, and injected into newborn mouse cortex. See also Supplemental Experimental Procedures and Table S2.

(B) Human nuclei+ cells expressed DCX and migrated into the cortex by 3 months post-injection (MPI). Blue: DAPI. Scale Bar: 100μm. Right panel is zoom of dashed rectangle in separate channels and merged. Scale Bar: 20μm. See also Figure S7.

(C-D) Quantification of lineage-specific marker histology at 2 (black), 4 (orange), and 7 (blue) MPI with d35 ML cells (C), or of subtype markers at 3 (black, blue) and 6 (orange, green) MPI with d50 aEB cells (D). Plotted as human cells near or dispersed from the injection site. Data represented as mean ± SEM.

(E) Histological analysis of human nuclei+ cells pre-labeled with *Syn*-YFP at 6 MPI that co-expressed (arrow) subtype markers. Blue: DAPI. Scale Bar: 20 μm. See also Figure S5.

(F) hPSC-derived neuron labeled by intracellular filling of neurobiotin (NB, green). Inset: *UbC*-RFP fluorescence of filled neuron 7 MPI. Scale bar: 20 μm; inset 5 μm.

(G) Traces of AP firing patterns of type I (left) and type II (right) hPSC-derived neurons upon near threshold (top) and superthreshold (bottom) current injection at 7 MPI. Scale bars: 50 mV and 100 ms. See also Figure S7.

(H) Left panel: traces of spontaneous PSCs recorded from hPSC-derived neurons at 7 MPI; upper right: BMI blocked PSCs with slow decay-time (arrow), and the remaining PSCs with fast decay-time (arrow head) were blocked by subsequent application of CNQX (lower right panel). Scale bars: 50 pA, 2.5 s and 0.2 s (dashed line) for zoomed traces.